# I. Introduction

Modulation of cell viability, morphology, adhesion, and proliferation at the bio-surface interface is pivotal to tissue engineering (*1-4*) and regenerative medicine (*5-7*). Previous studies show that surface chemistry plays primary role in controlling cellular behaviors; however, growing evidence indicates that physical structures are involved in this process by providing scaffolds and interacting with the functional assemblies on the cell membrane.

Surface topology at nanoscale encodes information that directs cell behavior (*8-13*). To decode the 3-d structural information cells are cultured on nano-scaled structures, such as nanoisland, nanopits, nanoneedle, nanopost. In addition, cells are also grown on random structures such as nanofibers or metal surface that mimic native structure of extracellular matrix.

Nano-scaled islands of height ranging from 13-nm, 35-nm, to 95-nm are derived from polymer demixing technique. Cell morphology, cytoskeletal organization, formation of focal adhesions, and gene expression at genomic scale have been obtained for various cell lines, including endothelial cells, fibroblasts, and mononuclear blood cells. In general increased cell adhesion, proliferation, long-term adhesion, cytoskeletal organisation, extracellular matrix remodelling was observed with 13-nm nanoisland (*14*). Reduced cell adhesion, reduced cytoskeletal organization, and less extended cell morphology are

associated with 35-nm to 95-nm nanoislands (*2*). In general, 13-nm nanoisland is beneficial

and promotes better spreading and proliferation of cells. Nanocolumns (100-nm in

diameter and 160~170-nm high) are fabricated by colloidal lithography. Decrease in

cytoskeleton organization is observed with human fibroblasts (hTERT-BJ1) cultured on the

nanocolumns (*15*).

Nanorods and nanoposts seem to inhibit cell proliferation and adhesion. Zinc oxide

(ZnO) nanorods are obtained from the solution-based hydrothermal growth method. Less

cell adhesion and lower viability of NIH 3T3 fibroblasts, umbilical vein endothelial cells,

and capillary endothelial cells are observed when culturing on ZnO nanorods (*16*). The

needle-like silicon nanoposts reduced cellular proliferation of fibroblasts (*17*).

Cells are grown on randomly deposited nanofibers that mimic the porous structure of

ECM. A 3D nanofibrillar surface composed of polyamide nanofibers can promote the

proliferation and self renewal of mouse embryonic stem cell (*18*). Mesenchymal cells are

cultured on chemical vapor deposition synthesized Si nanowires. Death occur to cells

cultured on the larger diameter ($d \sim$ 400-nm) within a day, whereas cells grown on smaller

diameter ($d \sim$ 30 -nm) were alive more than 5 days (*19*).

Cardiomyoblasts have great relationship with coronary artery disease. In order to

provide effective treatment for coronary artery disease, the material creating the stent must

be flexible, supportive, capable of expansion, and biocompatible. Biocompatibility is the

property of not incurring a toxic or detrimental immunological response. Most stents consist of stainless steel. The current metal options are gold, tantalum wires, a shape memory nickel-titanium alloy, biodegradable and bioabsorbable polymers, and drug-eluting stent. However, these materials seem to incur high restenosis and thrombosis rates, and very expensive to fabricate (*20*). Diamond-like-carbon coating stent suggested that it made high degree of macrophage spreading release (*21, 22*). However, the current materials applied to cardiovascular stent still have disadvantages and caused necrosis to patients. Furthermore, few of people utilize metallic substrate to fabricate the uniform nanostructures to investigate the interaction of cardiomyoblasts and expect to apply to stent. Therefore, we through anodic oxidation on Al of TaN films to obtain nanodot arrays.

Nanotopography is associated with the adhesion and proliferation of cells. However, the exact topology and size range that promotes cell growth or causes cell death are yet to be determined. The uncertainty is due to the difficulties in the fabrication of nanostructure with sufficient homogeneity and broad size range.

Arrays of nanodots with defined diameter and depth can be fabricated by using aluminum nanopores as a template during oxidation of tantalum thin films (*23*). The pore size of aluminum oxide is controllable and uniformly distributed; the depth of dots depends on the voltage applied; thus, it can serve as a convenient mold to fabricate tantalum into a nanodot array of specific diameter and depth (from 5-nm to 200-nm). The structure

containing nanodots of uniform size could serve as a comparable nanolandscape to probe cellular response at the molecular level.

We have shown, in the previous report, that nanodots of diameter larger than 100-nm induced apoptosis-like morphology for NIH-3T3 fibroblast cells (*24*). The topography also prevents cell adhesion, reduces cytoskeletal organization, induced apoptosis and correlated gene expression, and reduces the formation of focal adhesions. However, it is yet to be determined what range of nanotopography is capable of promoting cell adhesion and cell growth. All these parameters are important in designing artificial implants such as cardiovascular stents. The current study was undertaken to better define the topology and size ranges that determines the life and death of culture cells, especially for cardiomyocytes.
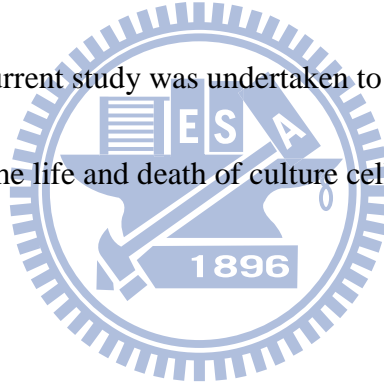
# II. Experimental Methods

2.1 *Cell culture*

To eliminate possible contamination of nano-micro particles, the cell culturing was performed in a class-10 clean room. H9c2 cells were cultured in Dulbecco's Modified Eagle's Medium complimented with 10% FBS and incubated at 37 °C, 5% $CO_2$.

2.2 *Chemicals*

Glutaraldehyde and osmium tetroxide were purchased from Electron Microscopy Sciences (USA). Anti-vinculin mouse antibody was purchased from Abcam (USA). Alexa Fluor 594 phalloidin, Alexa Fluor 488 goat anti-mouse IgG, were purchased from Invitrogen (USA). Trypsin was purchased from Sigma (USA). Bromodeoxyuridine drug and antibody were purchased from Millipore. Other chemicals of analytical grade or higher were purchased from Sigma or Merck. Anti-β-actin mouse antibody was purchased from Novus. High anti-plasminogen activator inhibitor-1 (PAI-1, *NOVUS*) rabbit antibody levels are associated with an increased risk of thromboembolic disease.

2.3 *Fabrication of nanodot arrays*

Nanodot arrays were fabricated as described previously (*23, 24*). A TaN thin film of 150 nm in thickness was sputtered onto a 6-inch silicon wafer followed by deposition of 3

µm-thick aluminum onto the top of a TaN layer. Anodization was carried out in 1.8 M

sulfuric acid at 5 Volts for the 10 nm nanodot array, or in 0.3 M oxalic acid at 25 Volts, 60

Volts, and 100 Volts for 50 nm, 100 nm, and 200 nm nanodot arrays, respectively. Porous

anodic alumina was formed during the anodic oxidation. The underlying TaN layer was

oxidized into tantalum oxide nanodots using the alumina nanopores as template. The

porous alumina was removed by immersing in 5 % (w/v) $H_3PO_4$ overnight. The dimension

and homogeneity of nanodot arrays were measured and calculated from images taken by

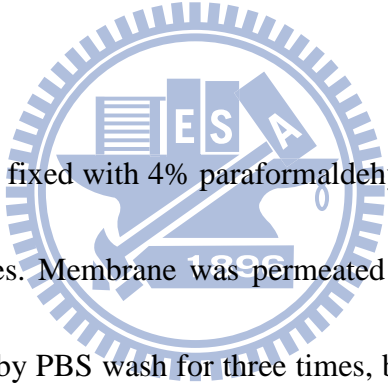JEOL JSM-6500 TFE-SEM.

2.4 *The cells viability assay.*

Cells were harvested and fixed with 4% paraformaldehyde in PBS for 30 min

followed by PBS wash for three times. And membrane was permeated by incubating in 0.1

% Triton X-100 for 10 min, followed by PBS wash for three times. The sample was

incubated with 4',6-diamidino-2-phenylindole (DAPI) and phalloidin for 15 min at room

temperature.
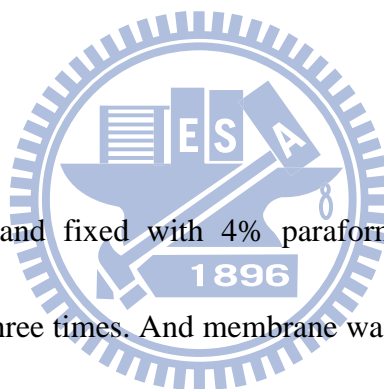
## 2.5 *Scanning electron microscopy (SEM)*

The harvested cells were fixed with 1% glutaraldehyde in PBS at 4 ºC for 20 minutes, followed by post-fixation in 1% osmium tetraoxide for 30 min. Dehydration was performed through a series of ethanol concentrations (10-min incubation each in 50%, 60%, 70%, 80%, 90%, 95%, and 100% ethanol) and air dried. The specimen was sputter-coated with platinum and examined by JEOL JSM-6500 TFE-SEM at an accelerating voltage of 5 keV.

## 2.6 *Immunostaining*

Cells were harvested and fixed with 4% paraformaldehyde in PBS for 15 min followed by PBS wash for three times. Membrane was permeated by incubating in 0.1 % Triton X-100 for 10 min, followed by PBS wash for three times, blocked by 1 % BSA in PBS for 1 hr, and PBS wash for three times. The sample was incubated with anti-vinculin antibody (properly diluted in 0.5 % BSA) and phalloidin for 1 hr, followed by incubating with Alexa Fluor 488 goat anti-mouse antibody for 1 hr followed by PBS wash for three times.

## 2.7 *Bromodeoxyuridine (BrdU) proliferation assay*

Cells were incubated with BrdU drug for 6 hours before harvest. Then, cells were harvested and fixed with 4% paraformaldehyde in PBS for 15 min followed by PBS wash

for three times. Membrane was permeated by incubating in 0.1 % Triton X-100 for 10 min,

followed by PBS wash for three times, and used 2N HCl to break the nucleic membrane.

Then, the cell was blocked by 1 % BSA in PBS for 1 hr. The cells incubated with 1% BSA

and BrdU (1:200) for 24 hours at 4°C. The sample was incubated with anti-

Bromodeoxyuridine antibody (properly diluted in 0.5 % BSA) and phalloidin for 1 hr.

2.8 *Western blot*

Cultured H9c2 cardiomyoblasts were lysed in 1X lysis buffer (Tris-Cl (Ph 7.4), NaCl,

EDTA, triton X-100, PMSF, proteinase inhibitor cocktail tablet (Roche), $H_2O$) and scraped,

and spun down at 12000 *g* for 2 mins at 4°C . Then, the supernatants were removed and

placed into new Eppendorf tubes and we used UV/OD to define the proteins concentration.

After we knew the proteins concentration, we used 4X sample buffer (glycerol,

β-mercaptoethanol, SDS, tris-Cl (Ph 6.8), bromophenol blue)  and lysis buffer to mix to

get 1μg/μL  protein. After piping, we heated (95°C) protein 3 mins, then cooled (0°C) its

3 mins, and repeated these steps twice. Proteins were separated on 10% SDS-PAGE and

transferred to PVDF membrans. Nonspecific protein binding was blocked in 5% milk at 4

°C,overnight. The membranes were blotted with specific antibodies as indicted for each

experiment in the blocking buffer at 4°C, overnight. Then the specific antibodies were

blotted with second antibody in the blocking buffer at RT, 1 hr. Chemiluminescent

detection was accomplished with Western Blotting Luminol Reagent , and oxidizing

reagent (U.S.A.) .

**2.9** *Quantitative real-time RT-PCR*

Total RNA was extracted from $1.8 \times 10^5$ cells using TRI-reagent (Talron Biotech)

according to the manufacturer's specifications. The RNA was isolated using chloroform

extraction and isopropanol precipitation. The crude RNA extract was immediately purified

with an RNeasy Mini Kit (Qiagen) to remove impurities and unwanted organics. Purified

RNA was resuspended in DEPC water and quantified by $OD_{260}$. The $OD_{260}$-to-$OD_{280}$ ratio

usually exceeded 2.0 at this stage. For cDNA synthesis, 1 µg total RNA was annealed with

1 µg oligo-dT, followed by reverse transcription using SuperScript® III Reverse

Transcriptase (Invitrogen) in a total volume of 50 µl. Between 0.2 and 0.5 µl of the reverse

transcription reactions were used for quantitative real-time PCR using SYBR Green I on an

iCycler iQ5 (Bio-Rad Laboratories). Cycling conditions were as follows: $1\times$ [5 min at

$95°C$] and $50\times$ [20 s at $95°C$, 20 s at $55°C$, and 40 s at $72°C$]; fluorescence was measured

after each $72°C$ step. Expression levels were obtained as threshold cycles (Ct), which were

determined by the iCycler iQ Detection System software. Relative transcript quantities

were calculated using the $\Delta\Delta$Ct method. The GAPDH, were used as reference genes and

were amplified from the same cDNA samples. The difference in threshold cycles of the

9

sample mRNA relative to the GAPDH, mRNA was defined as ΔCt. The difference between

the ΔCt of the untreated control and the ΔCt of the SMF-treated sample was defined as

ΔΔCt. The fold change in mRNA expression was expressed as $2^{\Delta\Delta Ct}$. The results were

expressed as the mean ± SD of six experiments.

Table 1. Primer sequences

| Gene | Forward sequence | Reverse sequence |
|---|---|---|
| GAPDH | gcctacctcatgggactgaa | acattctgccctttggtgac |
| Hsp27 | gagtggtctcagtggttcag | ccttccttggtcttaactgtg |
| Hsp60 | acaagtgatgttgaagtgaatg | atgcaggaattttaagtgctc |
| Hsp70 | cctacttcaacgactcgcag | cttcctcttgaactcctccac |
| Hsp90 | gtcttctctcgcttctcactt | vtatctgtgggaggggattct |
| beta-MHC | gcctacctcatgggactgaa | acattctgccctttggtgac |
| GATA-4 | agaaggcagagagtgtgtca | cagtgtggtggtggtagtct |
| PAI-1 | gaacgccctctattgtgccgaac | ctctgttggattgtgccgaac |
| ANF | tgggctccttctccatcacc | gccaaaaggccaggactgac |
| RAMP2 | ttactgctgctgttgctgct | aggaaagggatgaggcagat |
| RAMP3 | acctggtcgtgtcaaagtcc | ccacaccttccagatgacct |
| Bcl-2 | ctacgagtgggatactgg | gtgtgcagatgccggttca |
| Bax | ctgcagaggatgattgctga | gatcagctcgggcactttag |

# III. Results and Discussions

3.1 *Nanotopography modulated cell viability and proliferation of cardiomyolasts*

Nanodot arrays with dot diameters of 10-nm, 50-nm, 100-nm, and 200-nm were fabricated as described previously by anodic aluminum oxide (AAO) processing on tantalum-coated wafer (*23*). Diameters are 15±2.8 nm, 58.1±5.6 nm, 95.4±9.2 nm, and 211.5±30.6 nm for 10 nm, 50 nm, 100 nm, and 200 nm dot arrays, respectively (Figure 1A,1B). The average height was 11.3±2.5, 51.3±5.5, 101.1±10.3, and 154.2±27.8 nm, respectively. Dot-to-dot distance was 22.8±4.6 nm, 61.3±6.4 nm, 108.1±2.3 nm, and 194.2±15.1 nm, respectively (*24*) . Dimensions of nanodots were well-controlled and highly defined.

To evaluate the viability of cardiomyoblasts, H9c2 cardiomyoblasts were cultured on fabricated nanodot arrays and on flat wafer at the density of 2,000 to 5000 cells per square centimeter. Cells were harvested at 24 hr (day 1), 72 hr (day 3), and 120 hr (day 5) after seeding. To identify viable cells, DAPI staining was performed (Fig. 2). Immunostaining using anti-actin filament IgG was performed to verify the normal growth state for cells stained by DAPI (Fig. 3). Density of viable cells was obtained from composite pictures (Fig. 5). On day 1, most cells grew well and the cell densities were comparable to flat control, except that cells grew on 200-nm nanodots array exhibited 64.9 % reduction in cell number compared to flat surface. On day 3, increase in viable cells was generally observed

11

for cells cultured on flat, 10-nm, and 50-nm surface; however there is 53.7% and 72.6%

reduction in cell density for 100-nm and 200-nm nanodots array respectively. On day 5,

there is a general reduction in viable cells compared to day 3, except for cells grown on

50-nm nanodots. There are 20.9%, 33.6%, 44.2%, and 55.5% reduction of viable cells for

flat, 10-nm, 100-nm, and 200-nm nanaodots on day 5 compared to the flat surface on day 3.

The reduction of cell number for flat and 10-nm on Day 5 is apparently due to the over

growth of cells which occupied more than 90% of culture dish and has little to do with the

nanotopology. Although there is minor increase of viable cells grown on 100-nm and

200-nm on day 5 compared to day 3 and day 1, significant retardation of growth was

observed with cells grown on 100-nm and 200-nm dots array when compared to flat

surface.

Bromodeoxyuridine (BrdU) cell proliferation assay is a non-isotopic immunoassay for

quantification of BrdU incorporation into newly synthesized DNA of actively proliferating

cells. BrdU was applied to differentiate the newly proliferated cells from pre-existing

culture. Additionally, DAPI was used to stain the nuclei which represented total viable cells

(Figure 6). On day 1, maximum proliferation occurred for cells grown on 50-nm nanodots,

which is approximately 2-fold compared to flat surface. On day 3, significant proliferation

is still observed; however, the growth rate is reduced probably due to the saturation of

cells.

In summary, optimized growth occurred at 50-nm, on which maximum viability was maintained even when the cell density reached saturation. For flat and 10-nm nanodots, cardiomyocytes grew well, however, minor decrease in viability was observed on day 5 when cells were grown to saturation. Nanodots of 100-nm and 200-nm prevented viable growth of cardiomyocytes up to 53.7% and 72.6% reduction on day 3. Maximum proliferation occurred for cells grown on 50-nm nanodots, which is approximately 2-fold compared to flat surface.
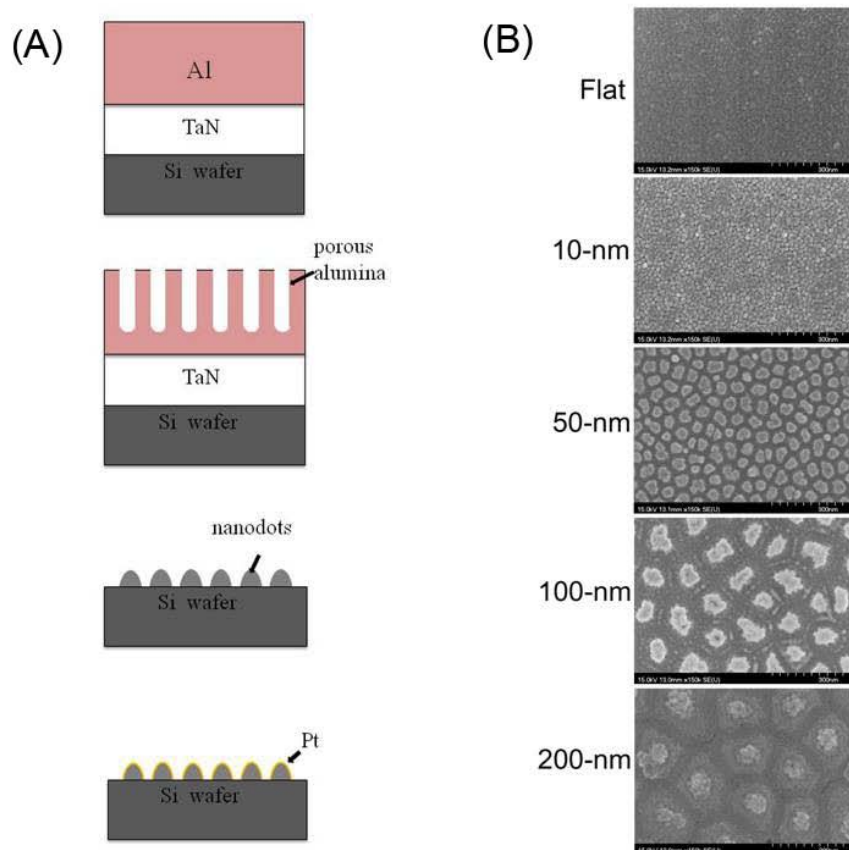


Figure 1. Tantalum-based nanodot arrays were fabricated by AAO processing. (A) Schematic representation for the fabrication of nanodot arrays. (B) High resolution scanning electron micrographs of nanodot surface: Flat, 10-nm, 50-nm, 100-nm,

13
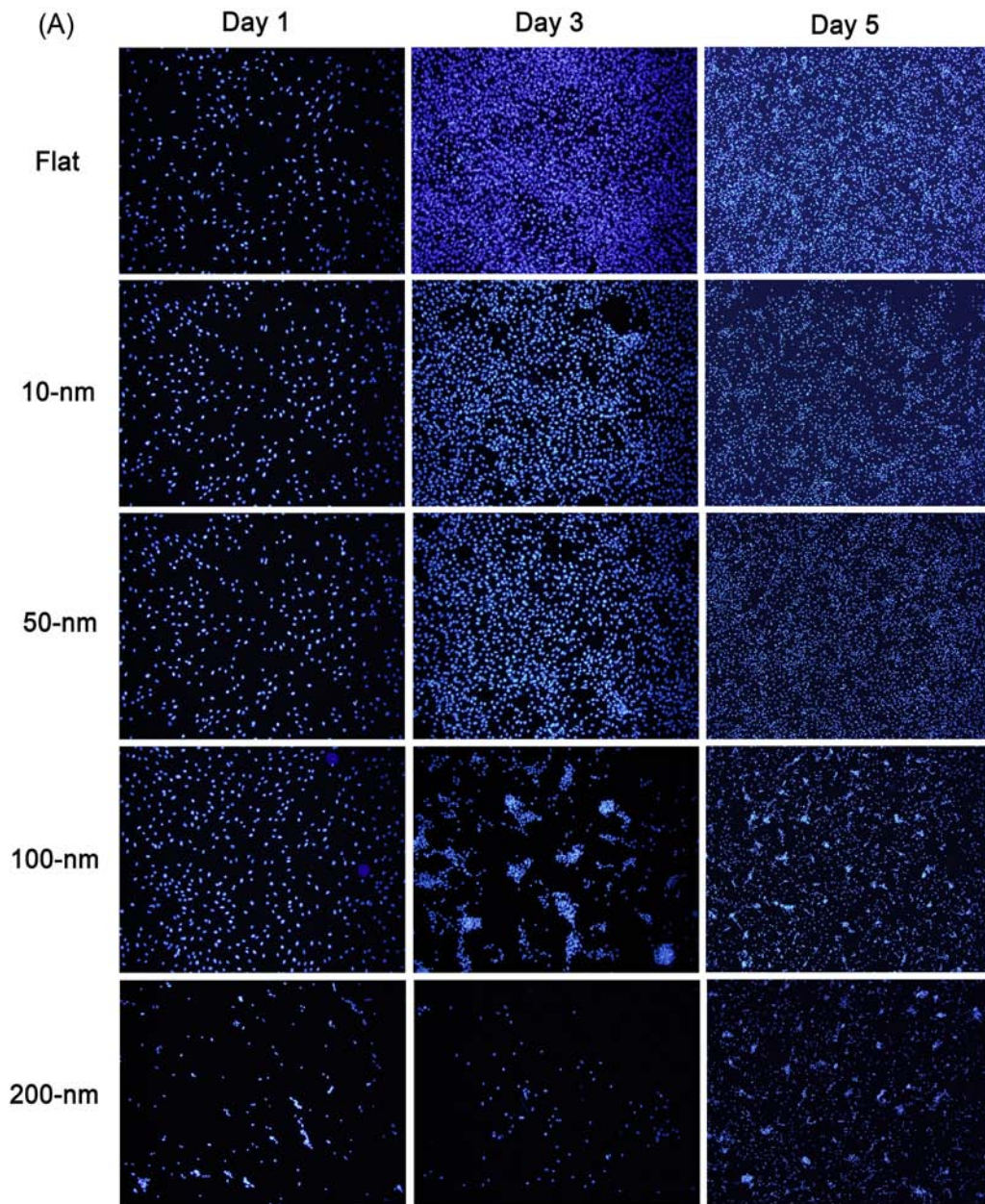
Figure 2. Immunostaining to show distribution of DAPI of cardiomyoblast cultured on nanodots arrays. The cell were seeded on flat, 10-nm, 50-nm, 100-nm, and 200-nm nanodots arrays.
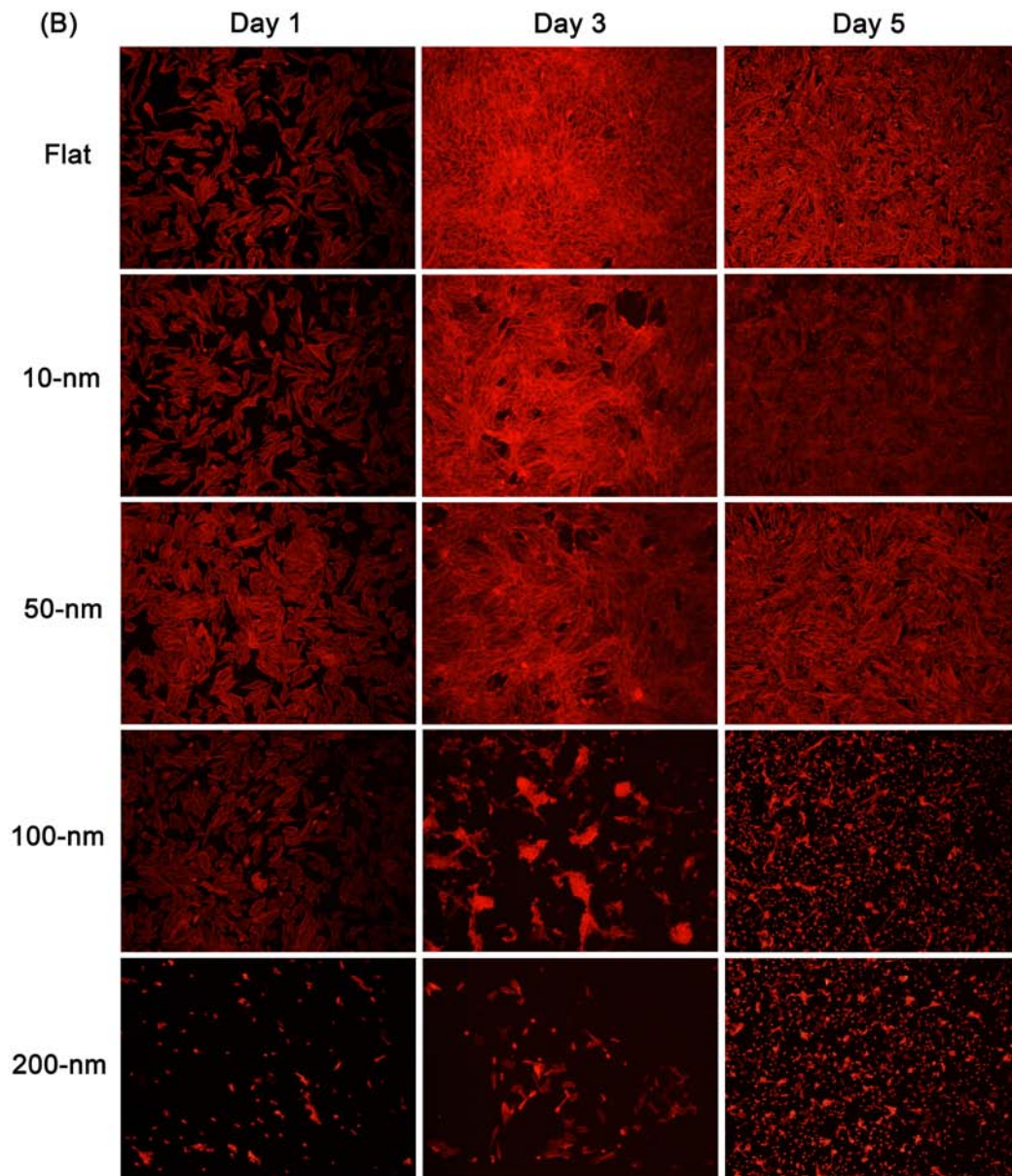
Figure 3. Immunostaining to show distribution of actin filament in cardiomyoblast cultured on flat, 10-nm, 50-nm, 100-nm, and 200-nm nanodots arrays. Cells were seeded on the arrays for 24 hours, 72 hours, and 120 hours before harvest.
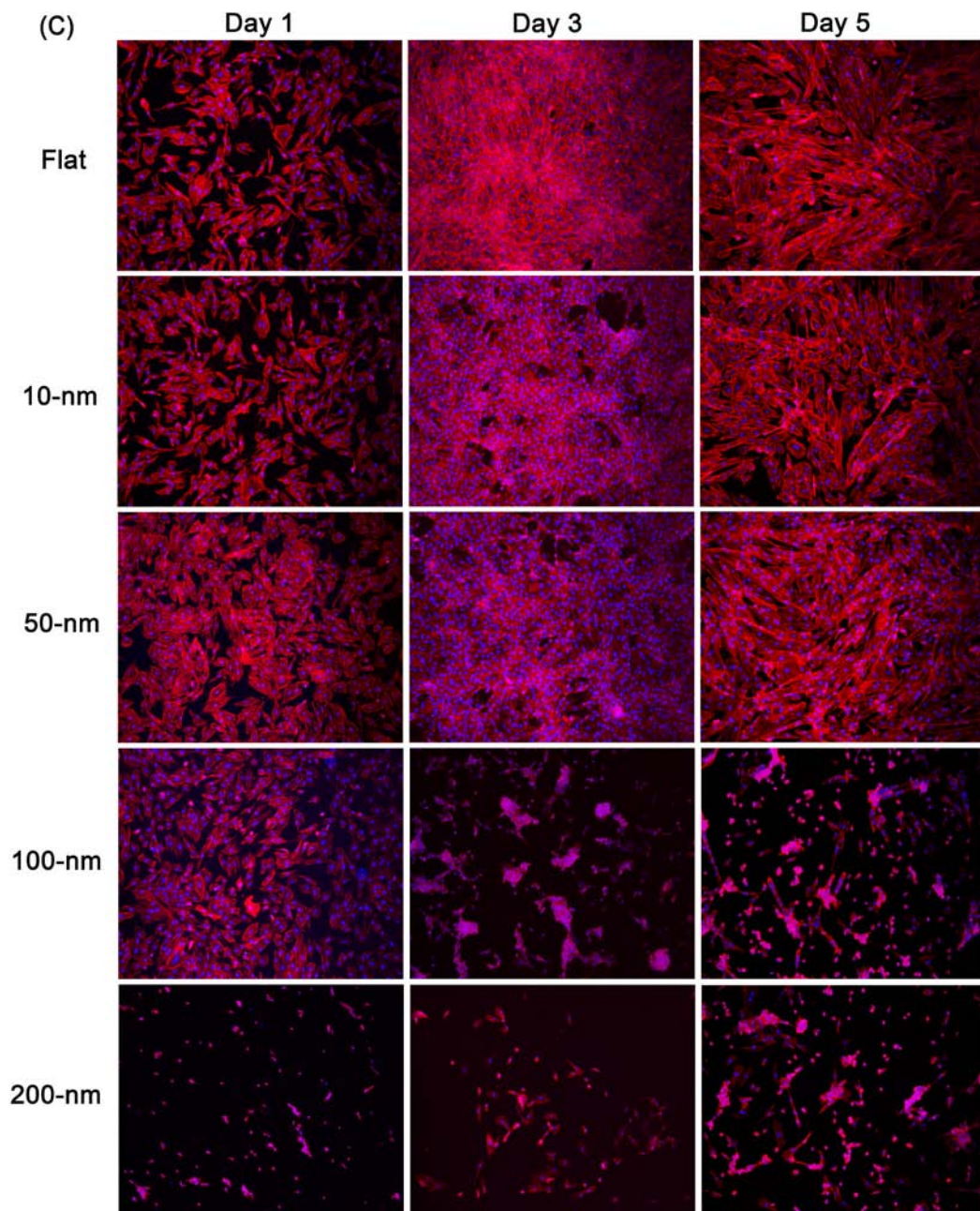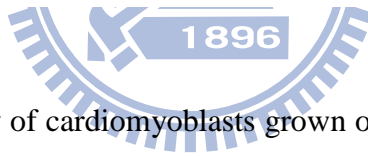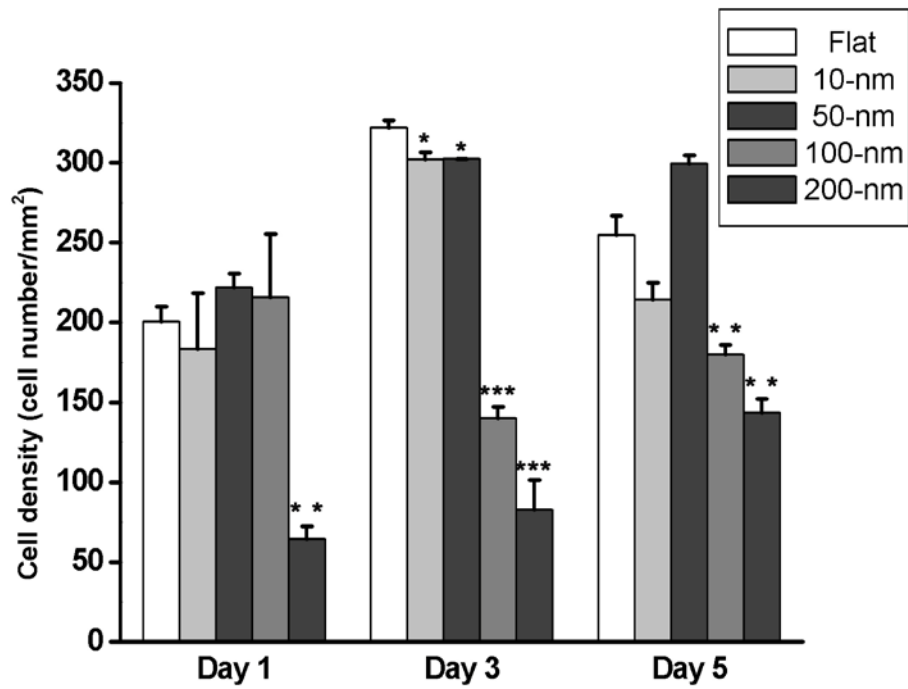
.

Figure 4. Immunostaining to show DAPI and actin filament in cardiomyoblast cultured

on flat, 10-nm, 50-nm, 100-nm, and 200-nm nanodots arrays.

Figure 5. The cell density of cardiomyoblasts grown on various sizes of nanodot arrays harvested on Day 1, 3, and 5. Cell density was derived from counting the number of cells double stained by DAPI and phalloidin (for actin filament). * =ANOVA, p<0.005
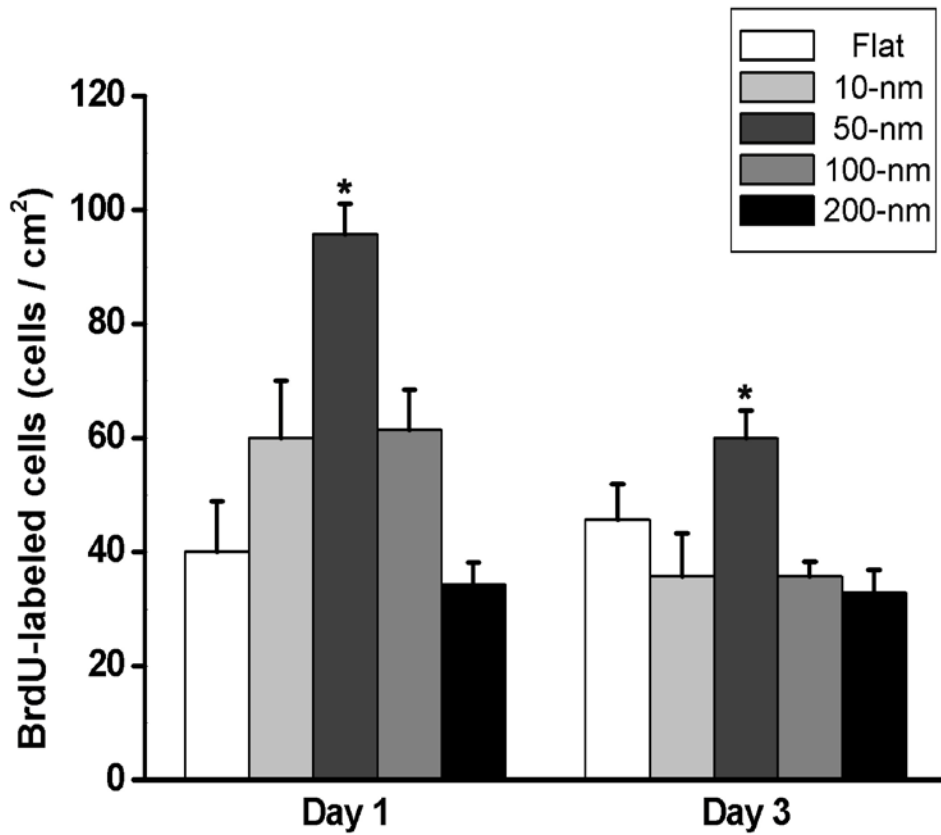
Figure 6. The statistics of proliferation ability of H9c2 cell, and the cell was incubated with bromodeoxyuridine drug for 6 hours before harvest. The sample was stained with mouse anti-bromodeoxyuridine monoclonal antibody. * =ANOVA, p<0.005.

3.2  *Nanotopography modulated morphology of cardiomyoblasts*

Morphology is an important index for cell growth. Flat and extended cells indicate healthy and proliferate growth. Nanotopography is known to modulate cell morphology of NIH-3T3 cells (*24*). Biochemical and genetic evidence indicated that apoptosis occurs to cells with abnormal morphology.

SEM was performed to examine the morphology of cells (Figure 7). Cells grown on the flat surface and 10-nm nanodot arrays exhibited flat and extended conformation during the course of 5 days. Cells grown on 50-nm nanodot array showed more extended morphology than flat surface with apparent larger surface area for each cell. Cells grown on 100-nm exhibited distorted morphology with shrinking surface area and increase in height. The apoptosis-like appearance and the reduction in surface area are mostly enhanced for cells seeded on 200-nm nanodots arrays.

The morphology of cells clearly varied when cultured onto different sizes of nanodot arrays. The variation was also dependent on incubating time. Surface area was measured and compared to cells grown on flat surface (Figure 8). On day 1, 2-fold increase in surface area for 50-nm compared to flat surface was observed. On day 3, significant increase of surface area for 10-nm and 50-nm was observed. The increase in surface area disappeared on day 5, probably due to the saturation of cells grown on culture dish. However, on day 5, cells grown on 100-nm nanodots begin to show significant reduction in size.

Formation of focal adhesions reflected by the attachment of filopodia and lamellipodia to the substratum indicates healthy growth for cultured cells (*28*). SEM images showed that the lamellar body of migrating cells, seeded on 50-nm nanodots arrays, exhibited wide and thick characters (Figure 9). Cells seeded on flat and 10-nm nanodots showed comparable lamellipodia. However, the cells seeded on 100-nm and 200-nm nanodos arrays are mounted with smaller size and narrow lamellipodia.

In summary, cells seeded on 50-nm nanodots showed most extended morphology, with largest surface area, most extended lamellipodia, and fastest growth rate. Cell grown on flat surface remained stable in culture dish, while apoptosis-like growth was observed with 100-nm and 200-nm nanodots with significant reduction in the surface area.
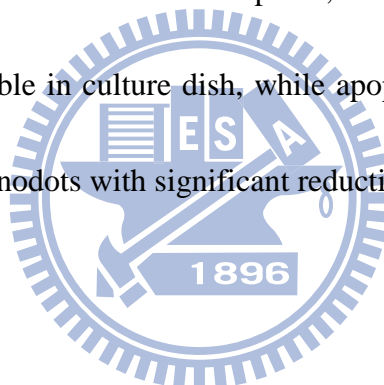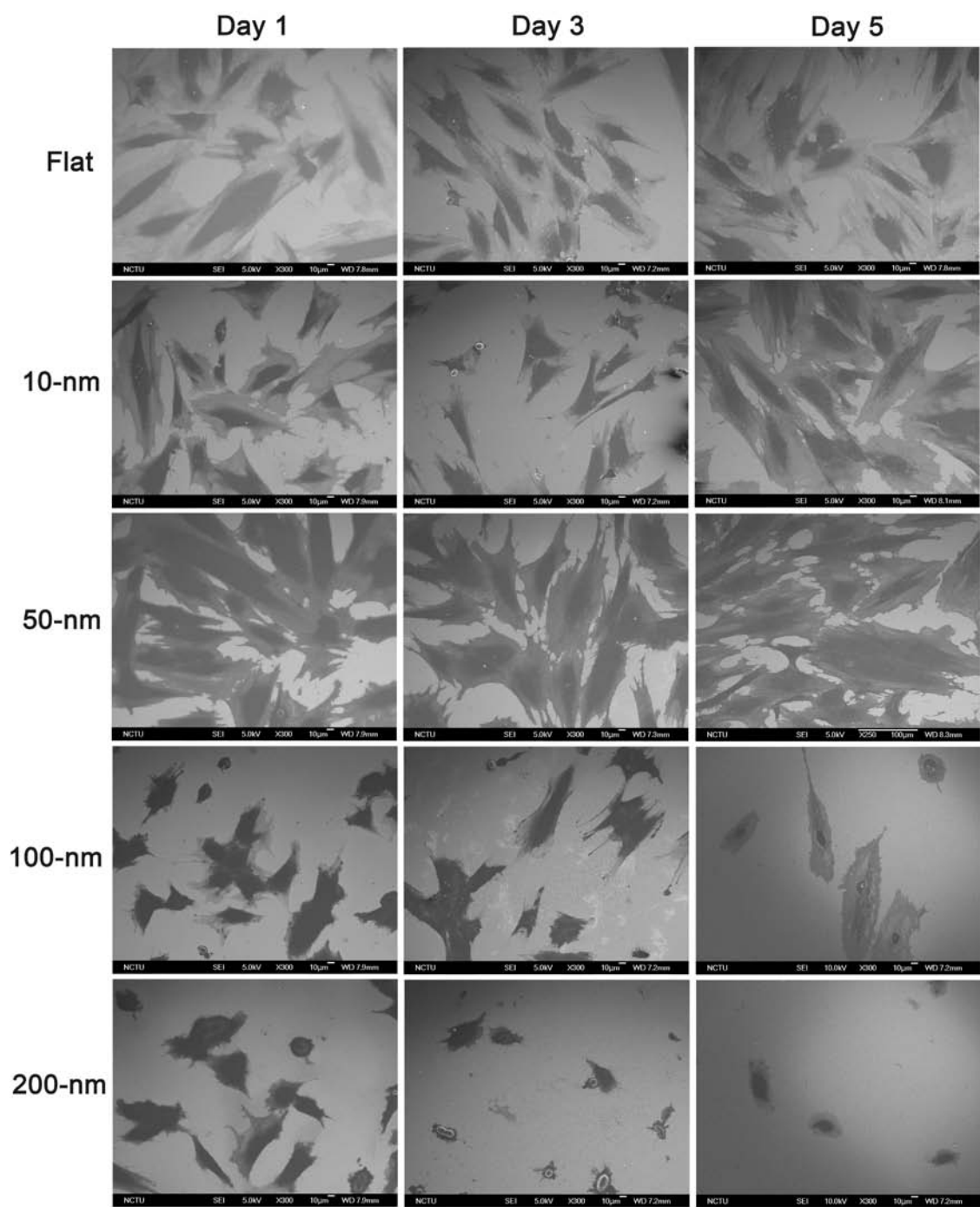
Figure 7. Morphology of H9c2 cardiomyoblast cultured on nanodots arrays. H9c2 cells were grown on Flat,10-nm,50-nm,100-nm,and 200-nm nanodot arrays for 1 day ,3 days, and 5 days and their morphology imaged by scanning electron microscopy.
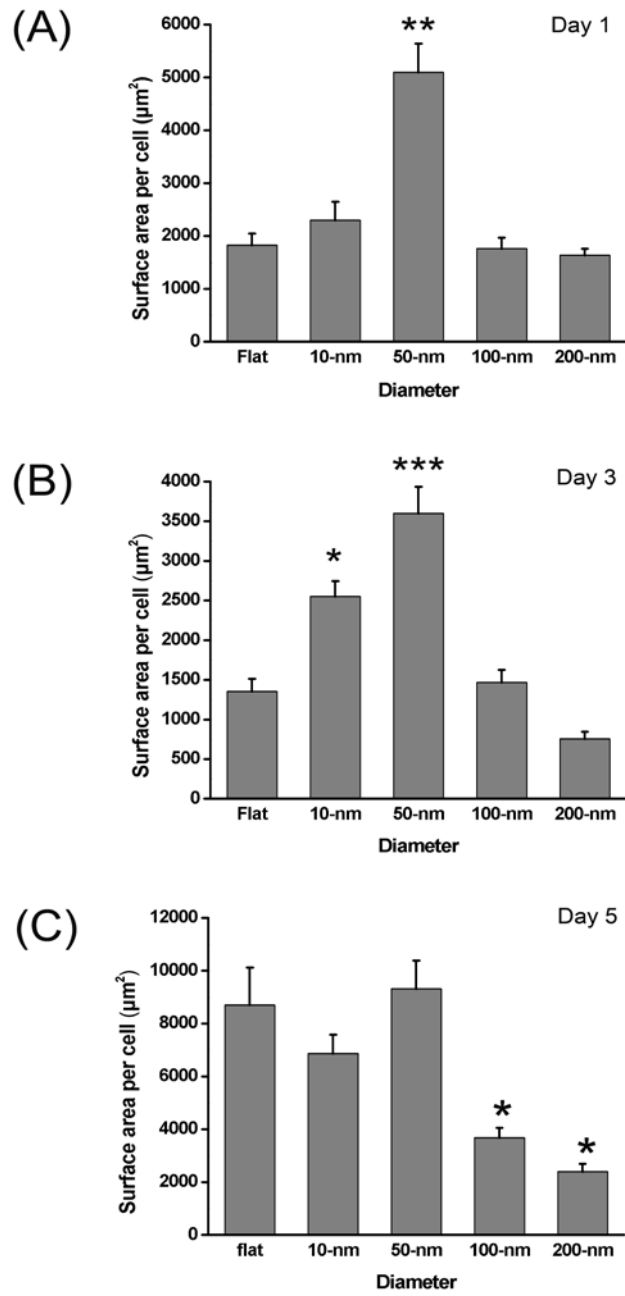
Figure 8. SEM statistics showed cells area. p<0.005. The surface area (per cell) seeded

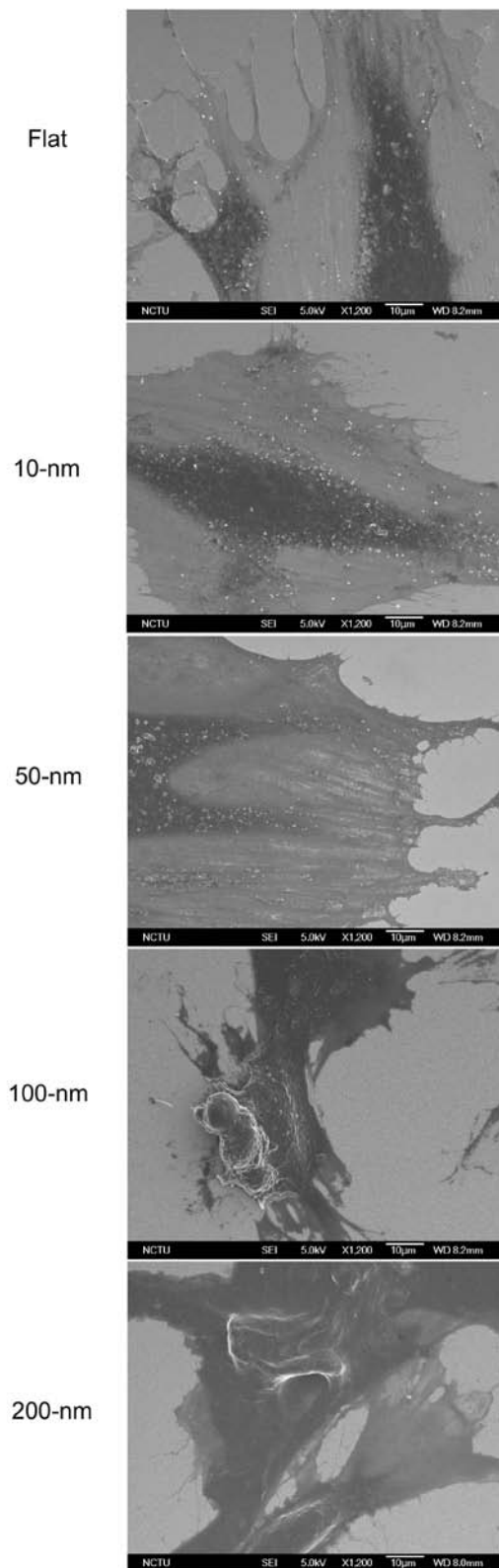on nanodots with control after (A) 1 day, (B) 3 days, and (C) 5 days seeded.

Figure 9. SEM images showed lamellipodia seeded on Flat, 10nm, 50nm, 100nm, and

200nm for 3 days before harvest.

3.3 *Nanotopography modulated cell adhesion and cytoskeleton organization of cardiomyoblats*

Topography and surface chemistry might share a common pathway to direct cell behavior. Focal adhesions are mediated by cell adhesion through receptor-ligand binding (*29, 30*).

To evaluate the role of adhesion molecules in nanotopography-induced apoptosis-like events, immune-staining specific to vinculin and actin filaments were performed to cells grown on nanodot arrays (Figure 10). Vinculin staining indicated the cellular formation of focal adhesions. Vinculin was detected and well distributed for cells grown on flat surface, and on the 10-nm, with highest density of vinculin occurred to cells grown on 50-nm nanodots arrays. The amount of vinculin staining decreased for 100-nm arrays and almost disappeared for 200-nm arrays. Well organized actin filaments were visible for cells grown on flat, on 10-nm, and on 50-nm nanodot array (Figure 11). This tight cytoskeleton arrangement was gradually lost for cells grown on 100-nm and completely disappeared for 200-nm arrays.

Immunostaining indicated that nanodots smaller than 50-nm promoted cell adhesion and cytoskeleton orgabization for cardiomyocytes. Best adhesion occurred at 50-nm. Nanodots of 100-nm retarded the formation of focal adhesions while 200-nm inhibited the organization of cytoskeleton (Figure 12).
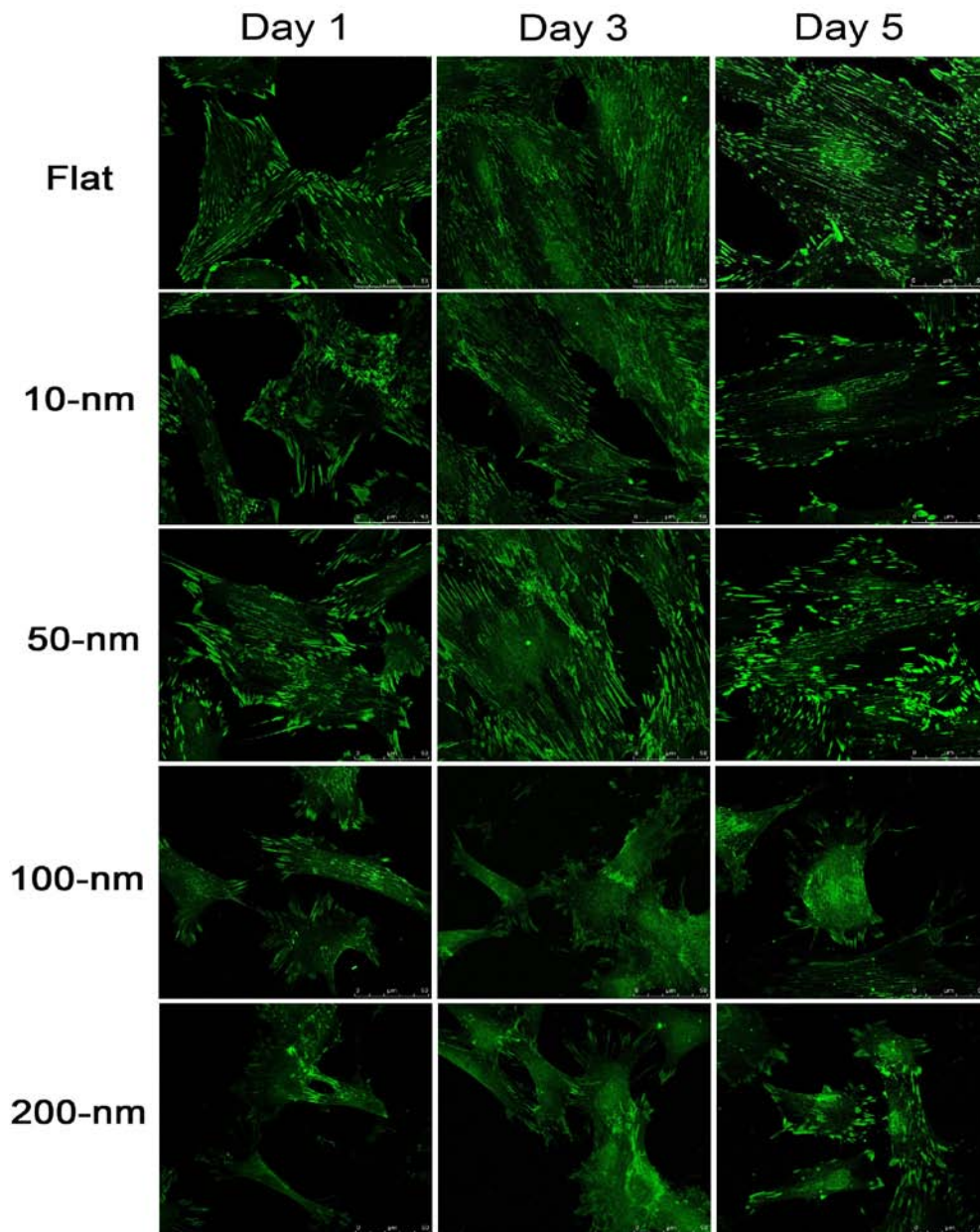
Figure 10. Immunofluorescent staining shows distribution of vinculin in H9c2 cells cultured on nanodots arrays. H9c2 cells were seeded on Flat, 10-nm, 50-nm, 100-nm, and 200-nm nanodot arrays for 1 day, 3 days, and 5 days. Scale bar = 50μm
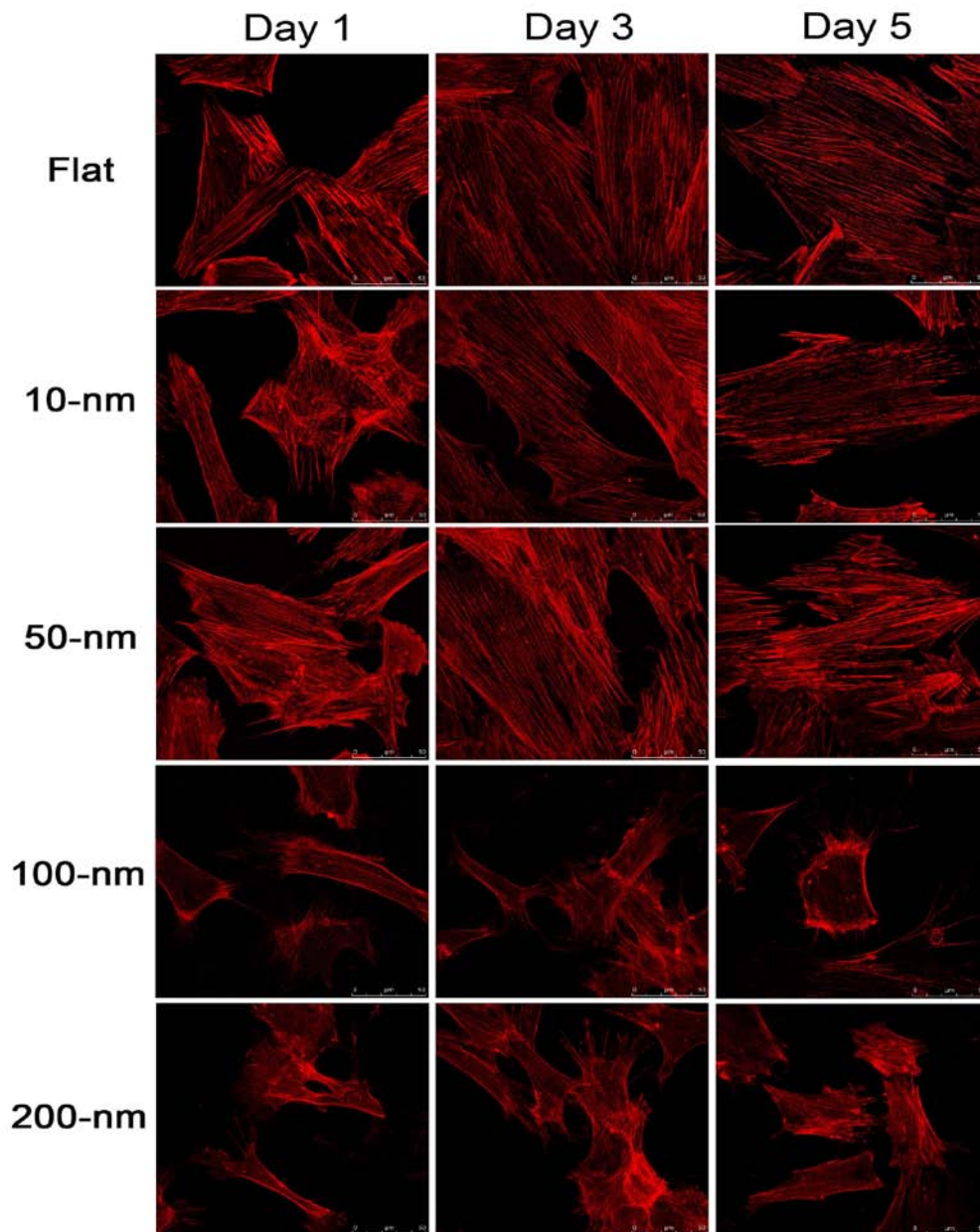
Figure 11. Immunofluorescent staining shows distribution of actin filament in H9c2 cells cultured on nanodots arrays. H9c2 cells were seeded on Flat, 10-nm, 50-nm, cultured on nanodots arrays for 1 day, 3 days, and 5 days. Scale bar =50μm.
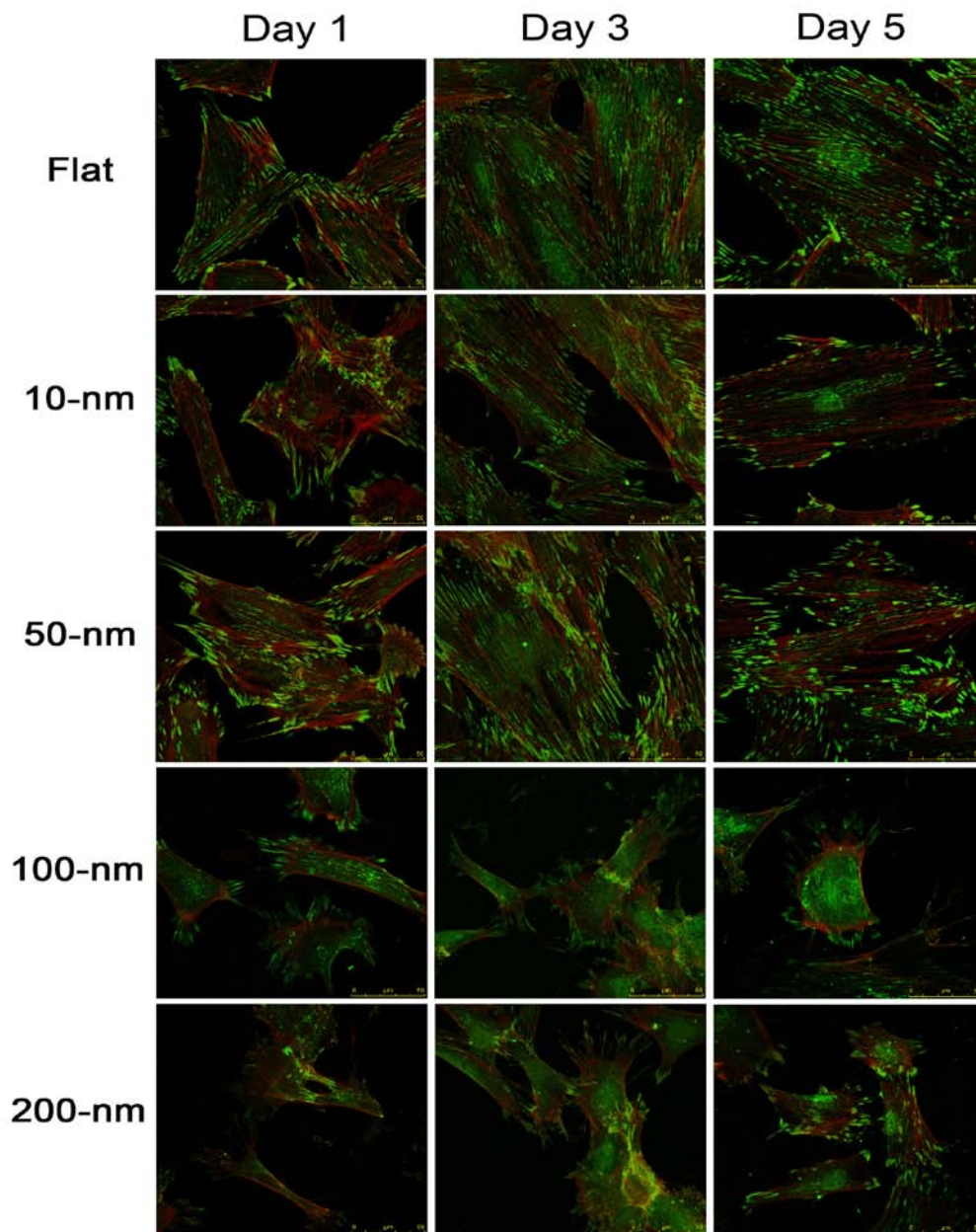
Figure 12. Immunofluorescent staining shows distribution of vinculin and actin filament in H9c2 cells cultured on nanodots arrays. H9c2 cells were seeded on Flat, 10-nm, 50-nm, 100-nm, and 200-nm nanodot arrays for 1 day, 3 days, and 5 days. Scale bar = 50μm

### 3.4 *Nanotopography influence cell survival mRNA expression*

Because many heat shock proteins involved the cell response in heart stress, we then tested the expression of Hsps in cells lysised from nanotopography. As shown in Figure 13, we found that mRNA levels of Hsp90 were significantly upregulated in 100-nm nanodots arrays expressing cells compared to 50-nm nanodots expressing cells, without evident mRNA level changes for Hsp70, Hsp60, and Hsp27.

Hsp90 has been identified as a signaling molecule in the activation of all the isoforms of nitric oxide synthase (NOS). The present study showed that Hsp90 induced by mild heat shock treatment can activate NOS enzymes in cardiac H9c2 cells, resulting in NO production, which regulates the respiration of the cells (*31*). The regulation of cellular respiration is directly related to many cardiovascular diseases. Periannan Kuppusamy group show that the Hsp90 induced during heat shock can activate NOS and increase NO production, resulting in the inhibition of respiration of the cardiac H9c2 cells (*32*).

Therefore, in the present data, the 100-nm nanodots arrays Hsp90 mRNA expression were significantly upregulated. We can conclude that 100-nm nanodots arrays cause the inhibition of respiration of H9c2 cardiomyoblasts (Figure 13).
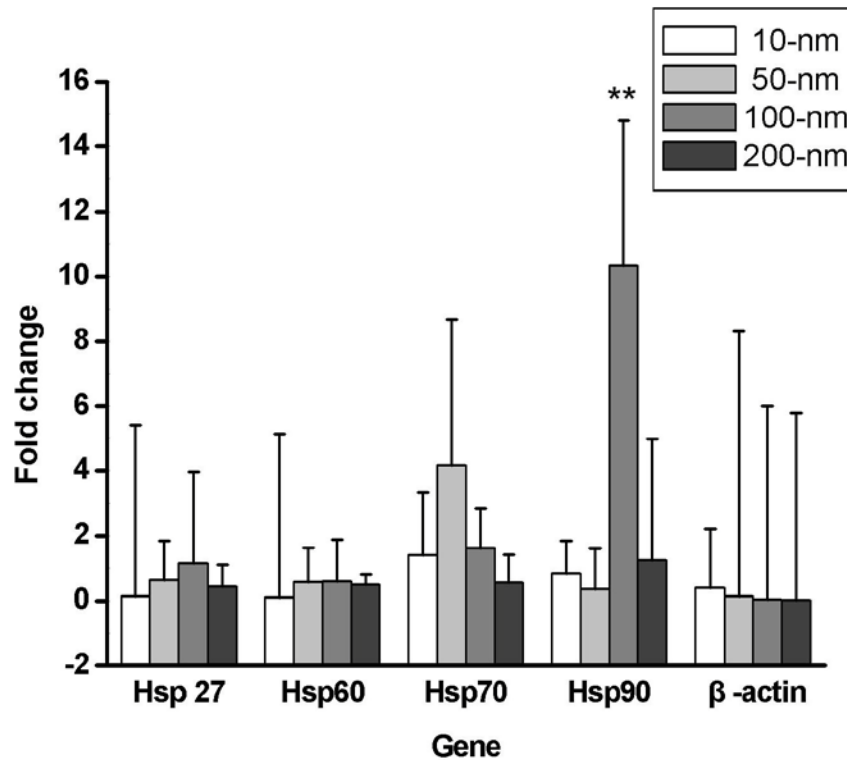
Figure 13. RNA was isolated from H9c2 cells stably transfected with flat, 10-nm, 50-nm, 100-nm, and 200-nm expression vector. Hsp90, Hsp70, Hsp60, Hsp27 and $\beta$-actin expression were monitored by RT-PCR analysis, respectively. (n=3, p<0.05)

## 3.5 *Nanotopography influence RAMPs expression*

Adrenomedullin (AM) is a peptide involved both in the pathogenesis of cardiovascular diseases and in circulatory homeostasis. The high-affinity AM receptor is composed of receptor activity–modifying protein 2 or 3 (RAMP2 or -3) and the GPCR calcitonin receptor–like receptor. RAMP2 is a key determinant of the effects of AM on the vasculature and is essential for angiogenesis and vascular integrity (*33*). We also focused on the nanostructures effect on the expression levels of Bcl-2 and Bax, two genes that play a key role in mitochondrial permeability and thus in apoptosis. We did not observed apparently variation in Bcl-2 and Bax mRNA expression after cardiomypblasts seeded on nanodots.

The expression profile of the 2 RAMP isotypes in H9c2 cardiomyoblasts was

determined by RT-PCR. The 100-nm nanodots arrays treatment increased the levels of RAMP2 and 3. Our finding may indicated 100-nm nanodots induced adrenomedullin and angiogenesis-like phenomenon (Figure 14).
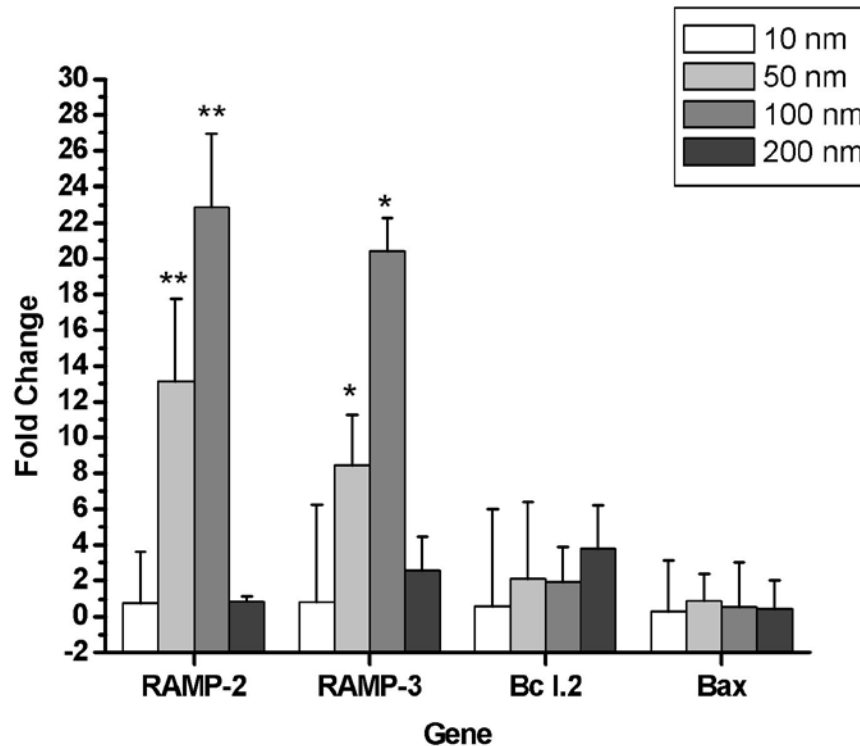


Figure 14. RNA was isolated from H9c2 cells stably transfected with flat, 10-nm, 50-nm, 100-nm, and 200-nm expression vector. RAMP-2, RAMP-3, Bcl-2, and Bax expression were monitored by RT-PCR analysis, respectively. (n=3, p<0.05)

3.6 *Nanotopography influence hypertrophy and fibrosis expression*

According to the study, aldosterone is directly implicated in cardiac hypertrophy and fibrosis. And it caused the up-regulation of the hypertrophy marker genes ANF, and β-MHC. Aldosterone has been reported to increase the expression of PAI-1, a factor that inhibits extracellular matrix-degrading metalloproteinases and promote fibrosis, in neonatal rat cardiomyocytes and in H9c2 rat cardiomyoblasts(*34*). The transcription factor GATA-4, a master regulator of cardiac genes, has been implicated in the transcriptional activation of genes encoding ANF and contractile proteins and in sarcomeric

reorganization in response to hypertrophic stimulation(*35*).

Figure 15 showed that the β-MHC mRNA expression of 50-nm and 100-nm nanodots arrays was significantly upregulated. We hypothesis this performance related to hypertrophic cardiomyopathy. The PAI-1 mRNA expression was increased that seeded on 100-nm nanodots array (Figure 15). We should conclude that 100-nm nanodots arrays may induce cardiomyoblasts fibrosis.
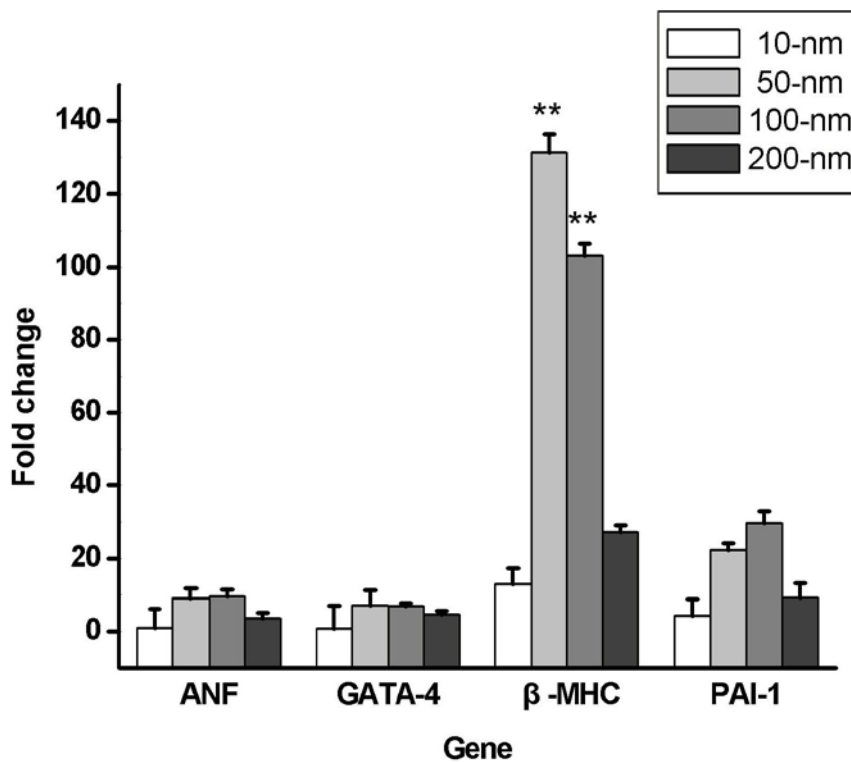


Figure 15. RNA was isolated from H9c2 cells stably transfected with flat, 10-nm, 50-nm, 100-nm, and 200-nm expression vector. ANF, GATA-4, $\beta$-MHC, and PAI-1 expression were monitored by RT-PCR analysis, respectively. (n=3, p<0.05)

3.7 *Nanotopography influence vinculin, PAI-1 protein expression*

. Myocardial infarction (MI) is frequently accompanied by fibrous changes and by left ventricular (LV) remodeling, which may result in the heart failure. Cardiac fibrosis, which is demonstrated by accumulation of extracellularmatrix (ECM), causes diastolic

dysfunction (*25*) . Plasmin, one of the serine proteases, is an active enzyme of the fibrinolytic system, and has a proteolytic activity as well. The fibrinolytic potential in the tissue is determined by balance between urokinase-type plasminogen activator (u-PA) and plasminogen activator inhibitor (PAI-1). PAI-1, which was shown to be expressed in mammalian cardiomyocytes (*26*), is implicated in the process of the cardiac remodeling by inhibiting activation of matrix metalloproteinases (MMPs) as well as plasmin generation. PAI-1 could inhibit interstitial proteolysis, especially in the infarct heart during the chronic phase, which determines the prognosis of MI patients. They have focused on the pathological role of PAI-1 in the cardiac repair. Experiments using mice deficient in PAI-1 suggests that increased expression of cardiac PAI-1 may contribute to the development of fibrous change after MI (*27*). The high expression of PAI-1, a factor that inhibits extracellular matrix-degrading metalloproteinases, could promote fibrosis.

We had investigated topography and surface chemistry might share a common pathway to direct cell behavior by immune-staining and RT-PCR. Vinculin and actin filaments were performed to cells grown on nanodot arrays. Cell survival, apoptosis, and hypertrophy and fibrosis mRNA expression were performed differently to cells seeded on different nanodots arrays. Now, we used western blot to quantitatively determine the vinculin and PAI-1 expression. According to our research, the protein performance of vinculin had the same trend with the immune-staining. The 50-nm nanodots arrays had upregulated expression

32

(Figure 16).PAI-1 performance also has the same trend with the RT-PCR result. Therefore,

we can hypothesis cells seeded on 50-nm nanodots arrays had high density of focal

adhesion and cells seeded on 100-nm nanodots had highest chance to promote fibrosis
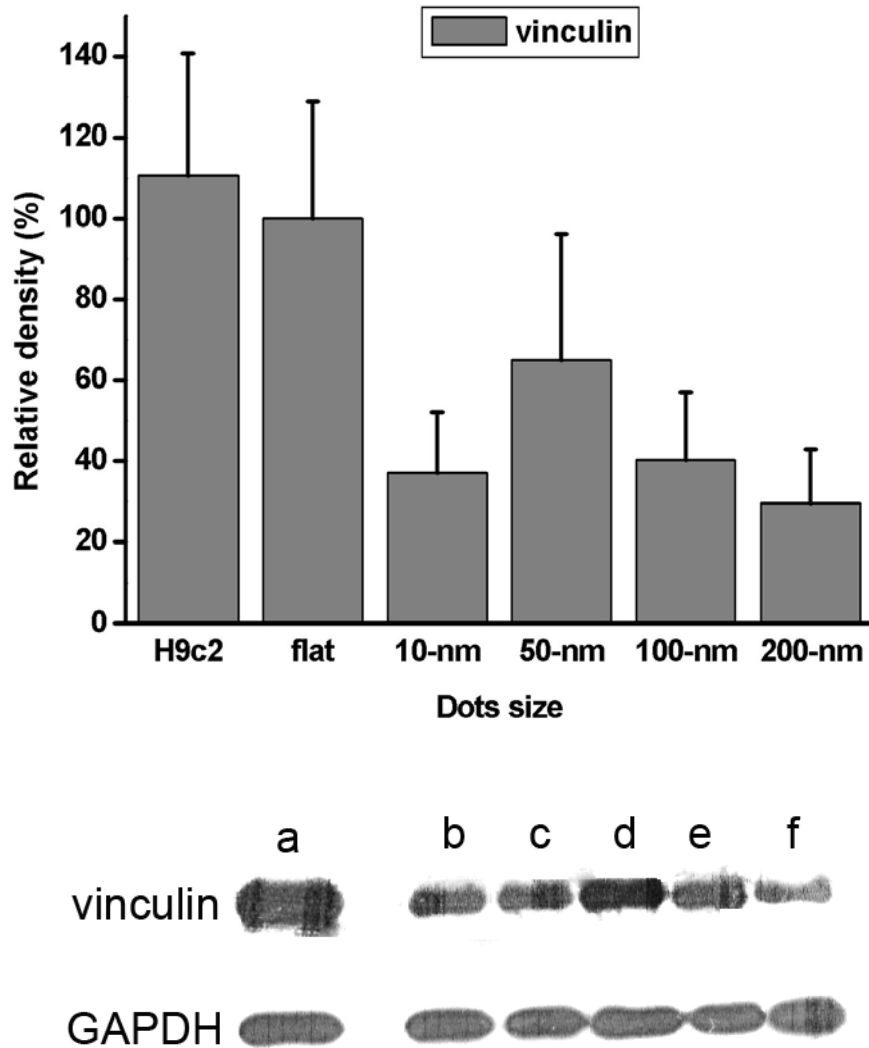
(Figure 17).



Figure 16. H9c2 cardiomyoblasts were collected after seeded on flask and nanodots for

72 hours and analyzed for the content of vinculin and GAPDH (as a control) by Western

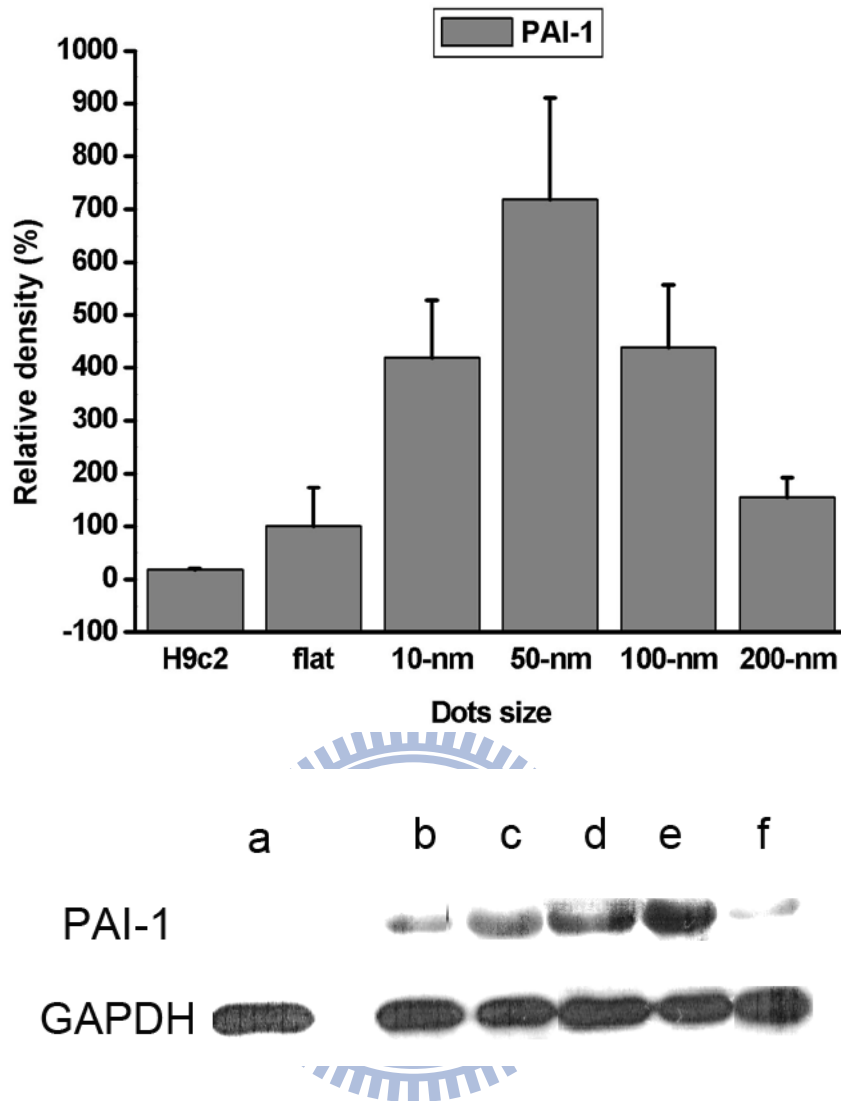Blot. a. H9c2 cardiomyoblasts, b.flat, c.10-nm, d.50-nm, e.100-nm, f.200-nm.

Figure 17. Cardiomyoblasts were collected after 72 hours and analyzed for the content of PAI-1 and GAPDH (as a control) by Western blot. a. H9c2 cardiomyoblasts, b.flat, c.10-nm, d.50-nm, e.100-nm, f.200-nm.

# IV. Conclusions

By adjusting the size of nanotopography we were capable of modulating the life and death of cardiomyocytes. In the case of nanodots array, the optimized growth occurred at 50-nm, which presented the highest viability, most extended morphology, best cell attachment, and highest proliferation. Such topography could be applied in the fabrication of implants. Implants with such surface are expected for better biocompatibility and suitable for long-term functioning in human body.

For 100-nm and 200-nm nanodots, the nanotopograhy retarded the cell growth and cell attachment, thus induced apoptosis in cells. RT-PCR showed that 100-nm nanodots can induce cardiomyoblasts fibrosis and cause inhibition of respiration of H9c2 cardiomyoblasts. Nanodots of 100-nm and 200-nm could be applied to surface of implants that purposely prohibit cell growth.

Here we show, by adjusting the size of nanodots, we are capable of modulating the life or death of cardiomyocytes. The current study will provide insights into the better understanding for the design of artificial implants and control of in vivo cell growth, such as stents.